Materials and Design 96 (2016) 106–114

Contents lists available at ScienceDirect

Materials and Design

journal homepage: www.elsevier.com/locate/matdes

3D printing of wood fibre biocomposites: From mechanical to actuation functionality

A. Le Duigou [a,*], M. Castro [b], R. Bevan [c], N. Martin [d]

[a] Polymer and Composites, Univ. Bretagne Sud, FRE CNRS 3744, IRDL, F-56100 Lorient, France
[b] Smart Plastics Group, Univ. Bretagne Sud, FRE CNRS 3744, IRDL, F-56100 Lorient, France
[c] ComposiTIC, Univ. Bretagne Sud, FRE CNRS 3744, IRDL, F-56100 Lorient, France
[d] Texilis, 2 Route de Bergues, 59210 Coudekerque-Branche, France

ARTICLE INFO

Article history:
Received 27 November 2015
Received in revised form 1 February 2016
Accepted 5 February 2016
Available online 6 February 2016

Keywords:
Natural fibres
Hygromorphic biocomposite
Fused Deposition Modeling

ABSTRACT

Natural fibres are increasingly used as reinforcements for thermoplastic composites. Additive manufacturing, also known as 3D printing, is a common material extrusion process using (bio)polymers reinforced with natural fibres. However, there is a lack of understanding of the effect of printing parameters on the mechanical properties involved in this new process, and more particularly in the case of Fused Deposition Modeling (FDM). Hygromorphic biocomposites represent a novel use of natural fibres for the production of original self-bending devices that actuate in a moisture gradient. By mimicking natural actuators and their bilayer microstructure adapted for seed dispersal, hygromorphic biocomposites take advantage of the hygro-elastic behaviour of natural fibres.

The FDM of wood fibre reinforced biocomposites leads to mechanical properties that are strongly dependent on printing orientation (0 or 90°) due to fibre anisotropy. Mechanical properties depend also on printing width (overlapping of filaments), with a lower Young's modulus than in the compressed samples. Indeed, printed biocomposites have a microstructure with relatively high porosity (around 20%) that conjointly leads to damage mechanisms but also water absorption and swelling.

The FDM of hygromorphic biocomposites enables a shift towards 4D printing since the material is able to evolve over time in response to an external stimulus. Typical microstructures achieved by printing could be used advantageously to produce biocomposites with a faster moisture-induced bending response compared to compressed samples.

1. Introduction

Thermoplastic polymers reinforced with natural fibres are increasingly studied as they provide an interesting range of specific mechanical properties in combination with a controlled environmental footprint [1] and a suitable end-of-life management. However, due to low the thermal resistance of plant fibres, most processing routes applied to these biocomposites, including extrusion, injection moulding, film stacking, vacuum bag moulding, etc., have a strong effect on the integrity of fibre cell walls [2,3].

Fused Deposition Modeling (FDM), a trademarked material extrusion process, has been attracting increased attention in the scientific community over the last few years due to its potential for reinventing the design process [4]. FDM enables quick and easy manufacturing of complex-shaped parts with no limitations due to geometry complexity. Moreover, it can be used in prototyping or tool manufacturing [5,6] for many applications such in as automotive engineering, aeronautics, construction or medicine [7]. FDM is currently the most commonly used additive manufacturing techniques because of the wide range of materials available from neat (bio)polymer to more recent (bio)composites [8].

The influence of processing parameters is currently being considered in several studies to promote the wider development of FDM. However, most of these studies are focused on pure polymers. Thus, when ABS filaments are overlapping, the tensile strength of the printed sample is improved compared with specimens that are overlap-free [9,10]. Another key parameter is the printing orientation, which highlights the anisotropic effect of printing [11]. Indeed, the longitudinal tensile strength of a 0°-oriented printed sample can be five times higher than in transverse counterparts [9]. FDM of natural-fibre composites is still rarely described in the literature. The only results available so far are more concerned with the global concept of 4D printing rather than materials research, even though this latter approach it is absolutely essential for such a technology [12].

4D printing is defined as the ability of 3D printed materials to actuate when an external stimulus is applied [13–15]. Basically, when natural fibres (wood, flax, hemp, etc.) are used as composite reinforcement, they

* Corresponding author.
E-mail address: antoine.le-duigou@univ-ubs.fr (A. Le Duigou).

http://dx.doi.org/10.1016/j.matdes.2016.02.018
0264-1275/

suffer from moisture sensitivity which degrades the mechanical properties and overall durability of the biocomposite material [16,17]. Nevertheless, moisture induced self-shaping wood [18–20] and natural-fibre biocomposites (called hygromorph biocomposites) have been recently developed [21], drawing inspiration from the structure/function relationship of natural materials such as observed through the seed dispersal mechanisms of pine cones [22,23]. These biocomposite materials exploit the hygroscopic behaviour of natural fibres for the design of new passive devices for solar tracking systems or responsive building skins. Indeed, the further development of applications remains an open question. The purpose of the present study is to propose a deeper insight into the effect of FDM parameters on the microstructure of a wood biocomposite and its consequences on hygro-mechanical properties. Finally, we show that it is possible to print hygromoph biocomposites with a dedicated bilayer microstructure, and test their actuation ability as a function of the microstructure induced by FDM.

2. Materials and methods

2.1. Materials

FDM filament is supplied by ColorFabb under the reference "Woodfill fine" with a diameter of 2.85 mm ± 0.1 mm. Woodfill fine filament is described as a blend of poly(lactic acid) (PLA) and poly(hydroxyalkanoate) (PHA) matrix, reinforced with recycled wood fibres. The fibre content, evaluated by chloroform dissolution of matrix and differential weighting, corresponds to a weight fraction of 15.2 ± 0.9%. This content is within the range given by the manufacturer (10–20 wt%), but appears rather low compared to other commercial products such as Laywoo® (40 wt% wood fibre) or EasyWood Coconut from FormFutura (40 wt% coconut fibre).

Unlike other studies on multimaterial printing [12], we chose a monomaterial to improve recyclability at the end of life and also reduce delamination between bilayers when the hygromorph biocomposites are printed.

2.2. FDM process

A Prusa i3 Rework 3D printer was used equipped with a 0.4 mm nozzle and heating plate allowing a maximum printing area of 19 × 19 cm^2. In this study, the 3D printer is controlled by Repetier host v1.0.6 software, combined with a Slic3r slicer. Printing parameters were set to a thickness of 3 mm. The temperature of the nozzle and heating plate was adjusted to 210 °C and 70 °C, respectively, and the printing speed was set at 18 mm/s. These parameters were found not to influence the properties of wood biocomposites, so they were deliberately chosen for the present study. Sample width (Fig. 1) can vary from 100 to 300%. This parameter has an important effect on biocomposite properties since it controls the overlapping of filaments and thus the internal cohesion of the printed specimen. Consequently, it deserves to be systematically studied.

Samples were printed with a rectilinear filling pattern oriented either 0° (longitudinal) or 90° (transverse) along the *x* axis without any contour (Fig 1). Tensile and actuation samples have the following geometry: L = 70 mm; W = 10 mm. To obtain a more accurate estimate of swelling, square samples were printed with an area of 1000 cm^3.

2.3. Characterization of mechanical properties

Tensile tests were performed on longitudinal (0°) and transverse (90°) samples with three biocomposite layers (≈1 mm) in dry and water-saturated state. Comparisons were carried out on compressed virgin filaments and printed samples, which were subsequently compressed on a heating plate (15 bars for 2 min at 210 °C) and then machine-milled with a previously defined geometry.

An MTS Synergie RT1000 traction machine was used with an extensometer to estimate Young's modulus. The tensile strain rate was set at 1 mm/min, and five samples were systematically tested for each determination.

2.4. Porosity

Porosity is obtained by comparing the density of compressed filaments (where porosity is assumed to be low) and printed samples. Porosity is calculated using Eq. (1):

$$\text{Porosity}\ (\%) = \frac{\left(\rho_{\text{compressed filament}} - \rho_{\text{sample}}\right)}{\rho_{\text{compressed filament}}} \times 100 \quad (1)$$

Measurements were carried out on 10 samples and the results were arithmetically averaged.

2.5. Water uptake and swelling

Five printed specimens were immersed in de-ionized water at ambient temperature, removed at selected immersion times and then wiped and weighed at room temperature (23 °C and RH = 50%) on a balance with a precision of 0.1 mg. The percentage gain W_t at time *t*, resulting

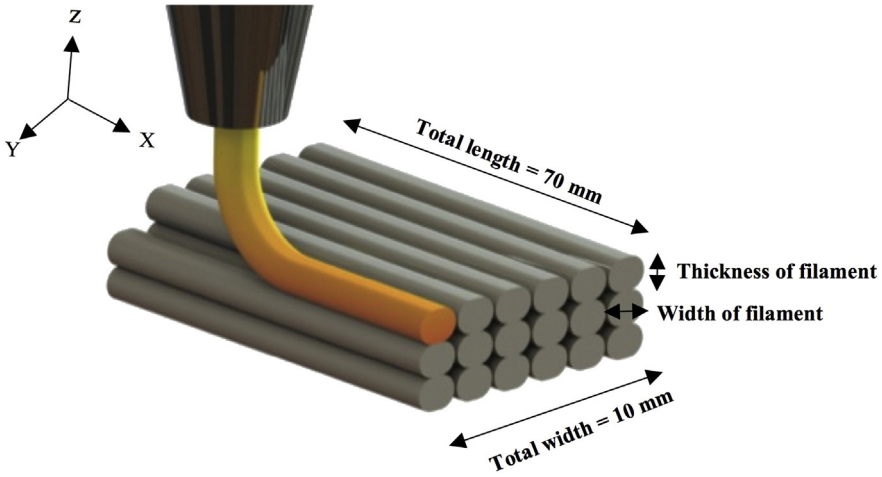

Fig. 1. Schematic representation of printed sample geometry for tensile tests and actuation.
Adapted from http://blog.capinc.com/2014/12/design-for-3d-printing-success/.

from water uptake, is determined by Eq. (2):

$$W\%_t = \frac{W_t - W_0}{W_0} * 100 \quad (2)$$

where W_0 and W_t denote, respectively, the weight of dry material (the initial sample weight prior to water exposure) and the weight of material after exposure to water. The maximum moisture absorption, M_∞, is calculated as an average value of several consecutive measurements that show negligible variation of water absorption.

Longitudinal (0°) and transverse (90°) swelling coefficients were obtained by measuring the evolution of geometry of a cubic sample (1000 cm^3). Five lines were plotted longitudinally and transversally to the printing direction to allow more accurate measurement by Vernier caliper. Five measurements along each direction were performed until constant swelling was attained. The swelling coefficients β are obtained from Eq. (3):

$$\beta\% = \frac{l_\infty - l_0}{l_0} * 100 \quad (3)$$

where l_0 and l_∞ denote, respectively, the length of dry material (initial sample length prior to water exposure) and length of samples after immersion in water.

2.6. Free curvature measurement

The bending curvature of the hygromorph wood biocomposite during immersion at ambient temperature in deionized water was estimated by periodically taking pictures of one side of the clamped sample. Image analysis was performed using ImageJ software (National Institutes of Health, USA). The curvature is measured by fitting the evolution of sample shape to a 'circle' function. Bending curvature is calculated using the radius of the fitted circle.

3. Results and discussion

3.1. Mechanical properties of biocomposites prepared by FDM

To improve our understanding of the effect of the printing process on the tensile behaviour and properties of wood-reinforced biocomposites, experiments were first carried out on the extruded filaments as received before printing as well as on 0° printed filaments, which were both compressed with heating plates. The longitudinal direction of printing (0°) corresponds to the direction of the raw filament extrusion when a hot press is used to manufacture samples with a reduced porosity (Fig. 3). Comparison is made between the raw compressed filaments and printed counterparts in the 0 and 90° directions (following the longitudinal axis of the sample). The mechanical behaviour and properties are shown in Fig. 2a, b and c.

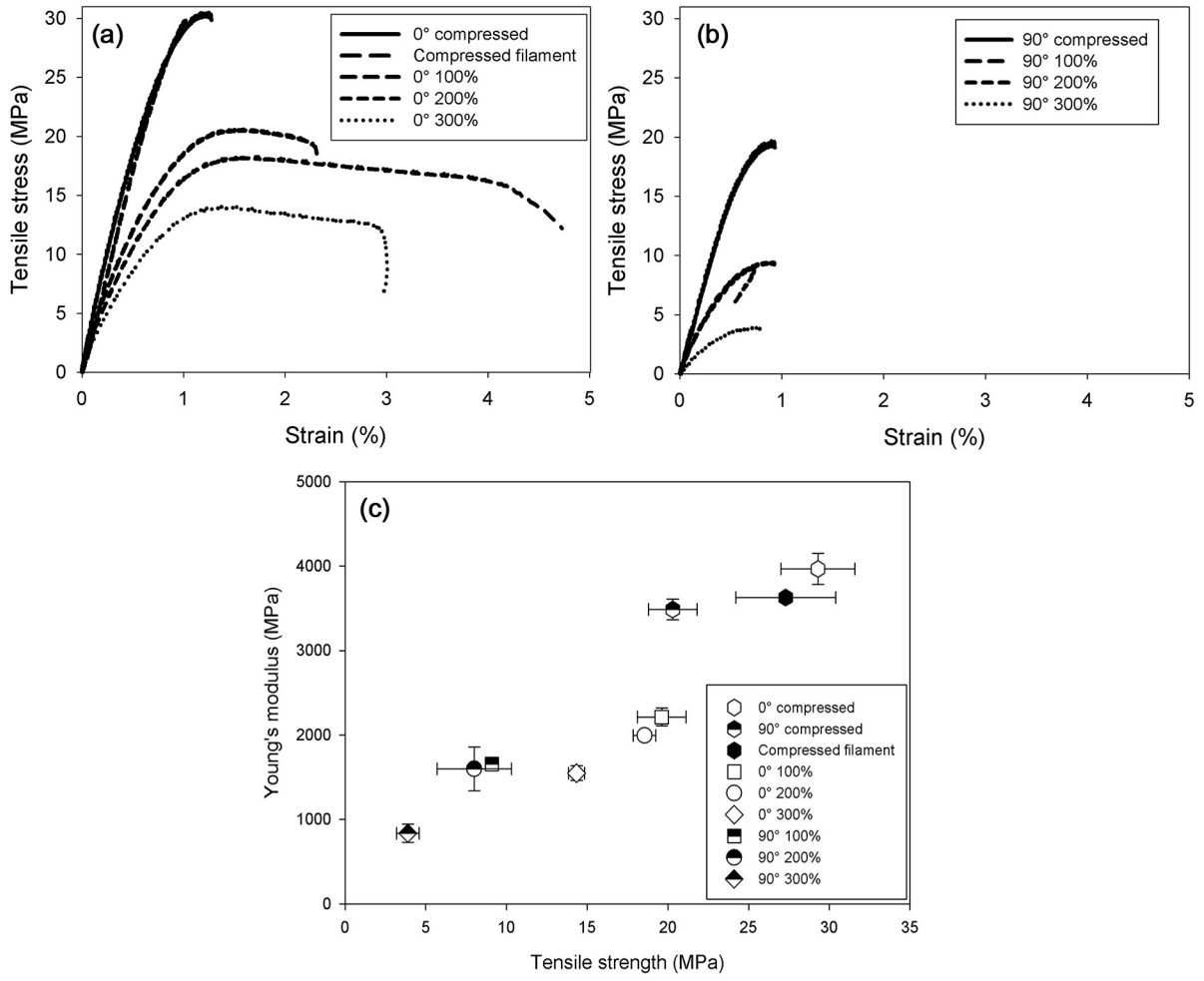

Fig. 2. Tensile behaviour of wood biocomposite made by FDM as a function of printing width (100, 200 and 300%) for (a): longitudinal printing direction (0°) compared to compressed samples; (b) 90° to the longitudinal direction. (c) Young's modulus as a function of tensile strength for different printing directions and widths.

The tensile behaviours of 0° printed/compressed samples and compressed filaments are clearly similar, with an almost elastic linear behaviour until the occurrence of brittle rupture (Fig. 2a). Their tensile properties are also closely similar (Fig. 2c). 90°-printed samples with additional compression do not exhibit any modification of the brittle behaviour (Fig. 2b). However, tensile stiffness and strength drop by about 20% and 35%, respectively, compared to their longitudinal counterparts (Fig. 2c). Therefore, it can be assumed that wood fibre orientation within the polymer matrix is brought about by the extrusion process (to produce raw filaments) rather than by the FDM process itself, mainly due to the lower shear stresses encountered. Considering there is little change of fibre orientation between compressed filaments and 0° printed/compressed samples, as shown by the mechanical test results, monitoring FDM direction opens the way to manufacturing wood biocomposites with customized mechanical properties (level, anisotropy, etc.). The mechanical properties obtained here are in the range of stiffness provided in the datasheet even if tensile strength is lower ($\sigma_{datasheet} = 46$ MPa and $E_{datasheet} = 3290$ MPa). The thermal degradation induced by our processing step could explain such a difference. Properties obtained for 3D printed/compressed samples and compressed filaments are in the range of polypropylene (PP)/wood 30% [24,25] and high-density polyethylene (HDPE)/wood 40% [26], but are lower than PHA/wood 20% ($E = 3820$ MPa $\pm$ 70 MPa and $\sigma = 65.80$ MPa $\pm$ 1.39 MPa [27] and PLA/wood 20% [28], all manufactured by extrusion and injection moulding.

Such differences could be due to several parameters such as the variety of wood used (biochemical composition, microstructure), the geometry of the filler (fibres, powder) and the processing parameters (shear rate, temperature). In addition, the wood-fibre reinforced biocomposites tested in the present study are made up of a blend of unknown percentages of PHA and PLA, including unknown additives, which complicates any straightforward comparison.

Printing thickness is linked with the pitch used by the printer, the filament length, the number of passes to print the part, the throughput and, finally, the printing time (Table 1).

From the data provided by the operator (printing width and thickness), the slicer calculates the amount of material required to print a pass, which then is converted into a filament length. The operator indicates the printing speed, and then the slicer again calculates the throughput and the printing speed at which the printer needs to operate.

According to the slicer software, the printing width is given as a percentage of the thickness of each printed layer (Fig. 1). Table 1 reports the results measured on the different samples with printing pitch varying from 100 to 300%. Here, the requested thickness is always 0.3 mm, so the theoretical printed pitch should be equal to 0.3, 0.6 and 0.9 mm for set values of 100, 200 and 300%, respectively. The wider the pass the higher the throughput and the lower the number of passes. We can estimate the percentage overlap by comparing theoretical values with printing width (Table 1).

For printed samples with a printing width of 100%, the real value of printing width is larger than the printing pitch. This involves a more cohesive microstructure with an overlap of 14.0% compared to samples prepared with printing width set at 200 and 300%. Indeed, these latter samples do not undergo any overlap (along the entire sample length), which creates limited contact area between each printed filament. Consequently, there is a higher porosity as shown by the SEM image and density measurements (Fig. 3). Only closed internal porosities are considered here.

Table 1
Printing parameters depending on printing width

Printing width	100%	200%	300%
Printing pitch (mm)	0.322	0.558	0.837
Throughput (mm^3/s)	1.567	2.715	4.072
Number of passes	310	179	119
Printing width (mm)	0.367 ± 0.01	0.557 ± 0.025	0.823 ± 0.025
Overlap (%)	13.9 ± 3.2	−0.2 ± 4.3	−1.6 ± 3.0

The porosity measured in the printed samples is very high compared to compressed samples (Fig. 3b, c and d), with an increase from 14.7 ± 1.4 to 15.5 ± 2.9 and finally 21.8 ± 1.2% for samples prepared with printing widths of 100, 200 and 300%, respectively, all in the 0° direction. Prior to printing, the initial biocomposite filament (Fig. 3a) showed a porosity of around 16.5%. Therefore, due to the lack of melting and blending pressure in the FDM device, the microstructure observed in the printed samples remains similar to the filament and is even exacerbated. The porosity within the samples is reduced by printing them along the 90° direction according to the long axis, falling to values of 8.4 ± 1.7, 11.1 ± 3.1 and 14 ± 1.2% for printing widths of 100, 200 and 300%, respectively, when compared to the 0° printing direction. Such differences may be explained by the closer packing of the printed filament once melted, due to a quicker pass between each printed filament, because of the sample geometry ($L = 70$ mm and $W = 10$ mm), which allows better mobility of the polymer chains.

Varying the printing width (100, 200 and 300%) induces a dramatic change of mechanical behaviour in the 0 and 90° printed samples (Fig. 2a and b) compared to the compressed counterparts. Unlike the 90° printed samples, 0° printed samples show a more ductile behaviour with increasing printing width, with a non-linear relationship between stress and strain until rupture. Compared with compressed samples having the same printing direction (0°and 90°), tensile strength is reduced by 30% and 50% for biocomposites prepared with 100 and 300% printing width, respectively, while the tensile modulus decreases by 50 and 65%. Such observation can be clearly explained in terms of the microstructure produced by 3D printing (Fig. 3c, d). The high amount of induced porosity promotes the onset of damage. The higher the porosity, the lower the mechanical strength properties.

Indeed, in contrast to the common thermoplastic processing route (extrusion, injection), the FDM process generates neither high moulding pressure nor high shear rate. Therefore, the material fails to develop high cohesion with strong interlayer interactions, as shown by the transverse tensile properties of the printed samples. In such cases, the adhesion between filaments that can occur during printing is mainly due to interdiffusion phenomena, which control the mechanical response of the biocomposite.

Biocomposite samples made by FDM thus exhibit poorer mechanical properties than biocomposites manufactured by extrusion, compression or injection moulding. Therefore, this novel technology allows the manufacture of parts having a complex shape, but nevertheless with moderate mechanical properties. Improvements could be obtained by developing suitable materials with low initial porosity and high fibre content. The fibre content actually represents a bottleneck since it may give rise to a drastic increase in the filament melt viscosity, thus hindering its use in current FDM apparatus.

3.2. Hygroscopic properties of biocomposites made by FDM

Beyond having a major influence on the mechanical properties of biocomposites, FDM also leads to a dramatic change of water uptake compared to compressed samples as illustrated in Fig. 4a. Indeed, compressed samples, which have a rather low porosity, absorb around 3 wt% (Fig. 4a) of water. This amount of water uptake is in the range of values found for biocomposites with similar amounts of plant fibres when using PLA or PHA as the polymer matrix [29, 30]. Increasing the printing width from 100 to 300% multiplies the water uptake by a factor of 5–10 compared with the compressed samples. Only a slight difference (a few %) can be observed between samples printed at 0 and at 90°. Water saturation of printed samples (after one month) occurs later than in the case of compressed counterparts (2 days), highlighting the modification of water transportation through the material. Slight differences of the

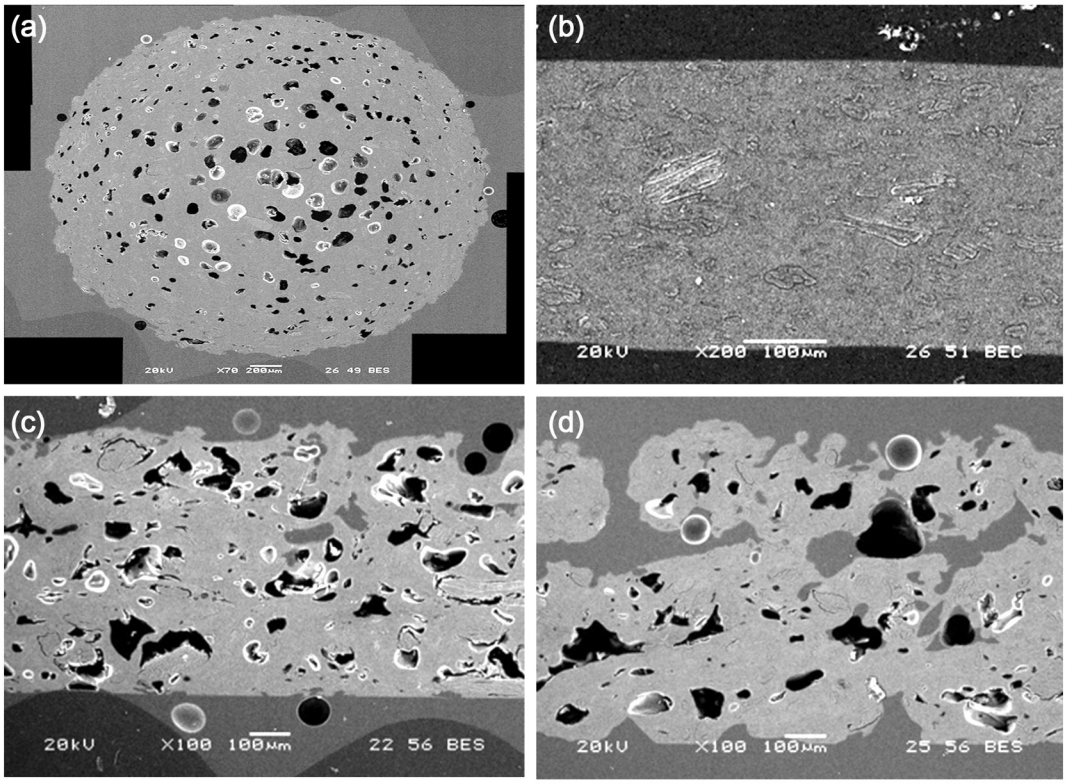

Fig. 3. SEM micrograph of cross-section of (a) raw filament, (b) compressed printed samples, (c) 100% and (d) 300% printing width samples. All samples are printed in the 0° direction. Scale bars in (a–c) indicate 100 μm.

time to reach saturation are observed between printing widths of 100%, 200 and 300%. Indeed, after 50,000 min (35 days), samples prepared with 200 and 300% printing width reach their saturation plateau, while, for 100% printing width, the water uptake still continues to increase (Fig. 4a).

As discussed in the previous section, the printing width and, to a lesser extent, the printing orientation induce a modification of biocomposite morphology with a high content of closed porosity. SEM images (Fig. 3) also reveal open cavities located on the surface of samples, but their role in water transport is here assumed to be negligible. Therefore, apart from the polar behaviour of wood fibres that essentially promotes water absorption and diffusion within biocomposites, high porosities induced by FDM could dramatically contribute to water transport. Late saturation is linked with the time required for the porosity to be filled with water. This sensitivity to water uptake also leads to an evolution of the dimension of pores while absorbing water (Fig. 3b). Both swelling ($\Delta RH = 50\%$) and maximal water uptake (Fig. 3b) depend on printing orientation. Indeed, we observe a swelling anisotropy that can be explained by the preferential orientation of anisotropic wood fibres within the sample along the longitudinal direction. Longitudinal swelling, i.e. 0° direction of printing, involves a slight swelling (around 0.2%) of the biocomposite, while transverse swelling increases to values of around 0.4% on compressed samples where porosity is assumed to be very low. Radial swelling of the biocomposite may appear rather low, but this is explained by the fibre content ($wf = 15.2 \pm 0.9\%$) and the constraint stress applied to wood fibres that reduces their swelling

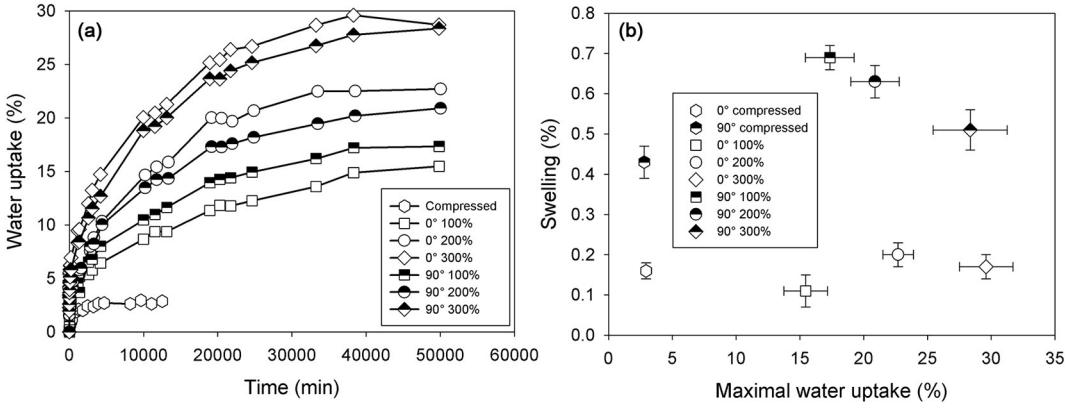

Fig. 4. (a) Water uptake of samples made by FDM as a function of time for different printing orientations and widths. (b) Water uptake versus swelling for different printing orientations and widths.

ability compared to free swelling [31]. Printed samples exhibit an increase of swelling compared to compressed counterparts, which highlights the impact of porosity on the swelling ability of biocomposites. However, samples prepared with 300% printing width show a relative decrease of around 30% of transverse swelling compared to samples prepared with 100% printing width. Porosity is not the only parameter that controls the swelling ability of biocomposites. The low transverse cohesion of samples prepared with 300% printing width, induced by the small contact area between printed filaments, may account for the observed reduction in transverse swelling.

The hygroscopic behaviour of biocomposites made by FDM influences their mechanical response, as can be seen in Fig. 4a and b, with the mechanical behaviour becoming more fragile compared to native biocomposites whatever the printing direction or width. Compared with compressed samples, we find that printing width (100, 200 and 300%) reduces the linear behaviour of water-saturated biocomposites for both 0 and 90° printing orientations (Fig. 5a and b). Compressed samples undergo a reduction in stiffness and strength of 10% and 30%, respectively, compared to dry samples (Fig. 5c). Such degradation mechanisms could depend on the weakening of wood fibre/matrix interfacial interactions due to water (VdW, A/B, thermal residual stress) [34], but may also lead to poorer wood fibre properties due to a plasticizing effect.

We observe a similar trend with different printed widths (100, 200 and 300%) in the 0° orientation, which therefore suggests a minor influence of biocomposite microstructure (porosity content) on moisture-induced degradation. This trend could be explained by the low volume fraction of wood fibres as well as their preferential orientation along the printing direction. Transverse properties (90°) are basically more sensitive to material cohesion, and undergo a reduction in stiffness and strength compared to 0° and compressed biocomposites, especially for samples prepared with 300% printing width. These samples have the lowest transverse cohesion but also the highest amount of porosity. In this case, the microstructure obtained via printing implies a lower resistance to water-induced degradation. Beyond the fibre/matrix and fibre degradation observed in the other samples, the weak cohesion between each filament for 90° printed samples with 300% printing width (Fig. 3d) has an effect on the overall durability of biocomposites.

FDM process can clearly produce biocomposites with poorer tensile properties compared to those manufactured by compression moulding. The microstructure and relatively high porosity induced by low moulding pressure can account for these trends by promoting damage mechanisms. Hygroscopic properties and water sensitivity are also altered by FDM, i.e. through high water uptake and swelling.

3.3. Hygromorph dynamic biocomposites

In nature, phenomena such as seed dispersal (involving pine cones or wheat awn) are driven by the effect of moisture gradient on an asymmetric bilayer microstructure [23]. The idea here is to use the anisotropic hygro-elastic properties of biocomposites to print a bilayer microstructure with differential elastic and swelling properties similar to the pinecone microstructure (Fig. 6a). Such kinds of biocomposites could actuate in response to a water gradient [12, 21]. Here, the printed bilayer structure is obtained by customizing the printing directions, 0 and 90° along the sample over many layers, while keeping similar wood biocomposite components to prevent delamination in between the layers. Once immersed, these biocomposite bilayers start actuating, i.e. bending themselves (Fig. 6b).

Unlike static biocomposites, which are developed to provide stiffness and strength, dynamic hygromorph biocomposites bring a novel

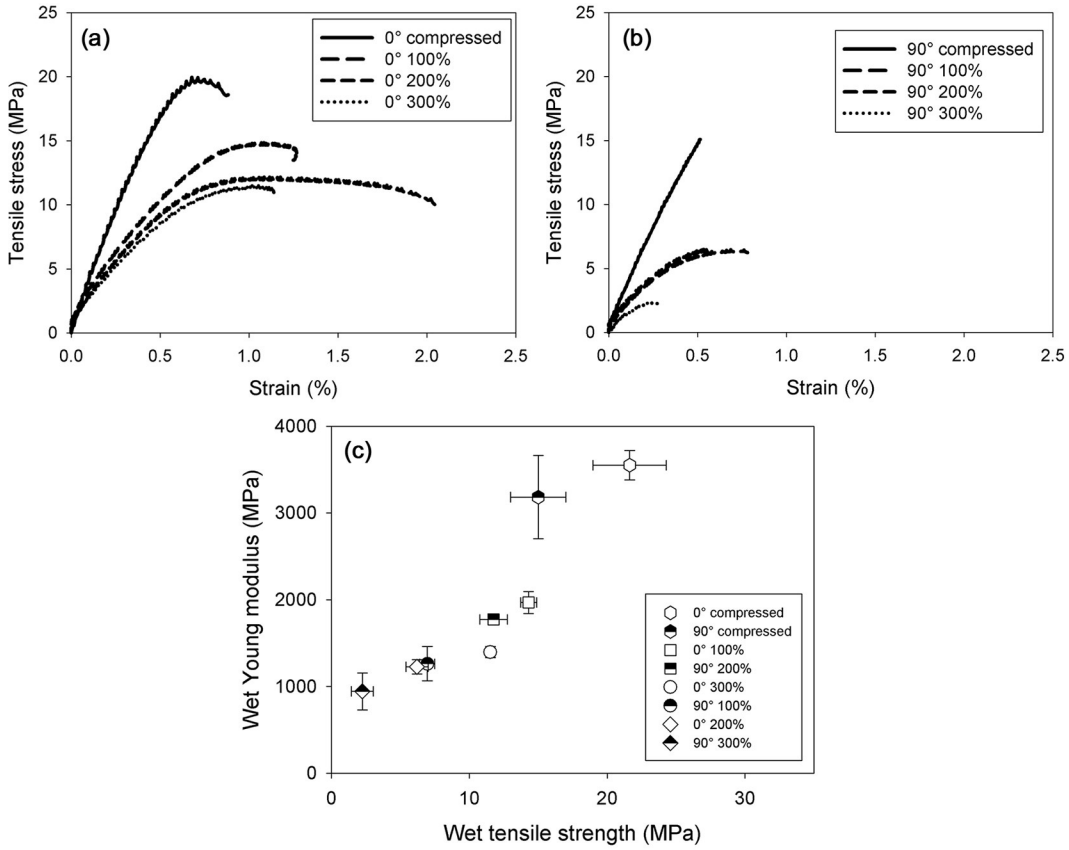

Fig. 5. Tensile behaviour of water-saturated wood biocomposites made by FDM as a function of printing direction: (a) 0° and (b) 90° to the longitudinal direction. (c) Young's modulus under wet conditions as a function of wet tensile strength for different printing directions and widths.

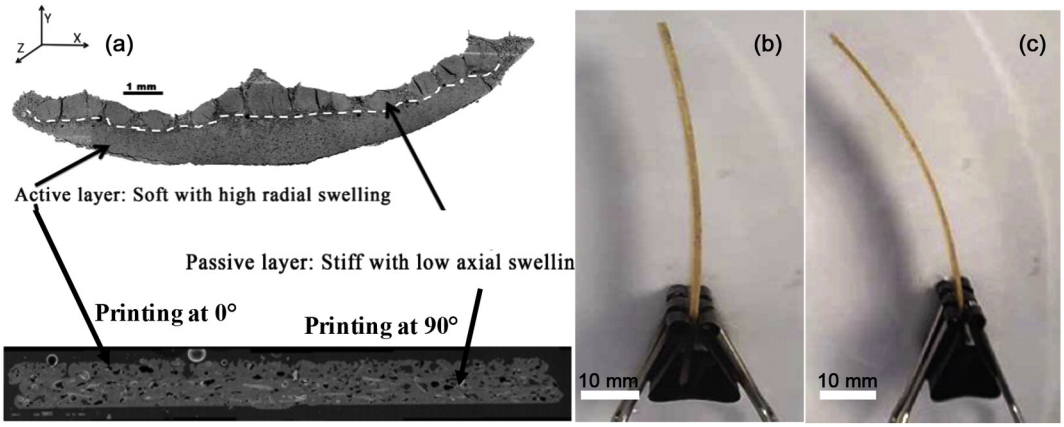

Fig. 6. (a) Principle of hygromorph biocomposite design based on the bioinspiration paradigm. Example of hygromorph biocomposite made by FDM (b) before and (c) after immersion.

functionality to biocomposites: self-shaping actuation. Such a material arrangement, i.e. a biocomposite bilayer actuated by a water gradient, can be well described in terms of the bi-metallic theory proposed by Timoschenko [21,32] using Eqs. (4) and (5), so it may be considered as programmable [33]:

$$\Delta\kappa\alpha = \frac{\Delta\beta\Delta\varnothing f(m,n)}{t} \tag{4}$$

$$f(m,n) = \frac{6(1+m)^2}{3(1+m)^2 + (1+mn)\left(m^2 + \frac{1}{mn}\right)} \tag{5}$$

with $m = \frac{tp}{ta}$, where *tp* and *ta* are the passive layer and the active layer thicknesses, respectively. Here, the active layer is considered as a transversally printed layer (90°), where swelling ratio is maximal in the longitudinal direction of the sample, while the passive layer is longitudinally printed (0°). Then $n = \frac{E_p}{E_a}$ where E_p and E_a are the Young's moduli of the wet passive and active layers, respectively. $\Delta\beta$ is the differential hygroscopic expansion between the active and passive layer. $\Delta\varnothing$ is the humidity rate difference between the immersion and the storage state. The differential expansion is set at $\Delta\varnothing = 50\%$, since storage steps are performed in a humidity- and temperature-controlled room (RH = 50%). Finally, *t* is the total thickness of the sample (active and passive layers). The change in curvature is calculated from Eqs. (4) and (5) as a function of layer thickness and hygro-elastic properties as evaluated in the previous section according to the printing thickness (i.e. compressed, 100, 200 and 300% printing width). An optimal *m* ratio of around 2 can be found for all the printed and compressed systems. Taking into account the experimental data and following the predictions of bimetallic theory, 100% printing width samples show higher curvature values, K, of around 0.012 mm^{-1} (Fig. 7a) compared to other printed systems and compressed samples. This variance has already been observed by Correa et al. [12] on wood biocomposites: the denser the grain, the smaller the folding angle. As discussed above, FDM process can provide a range of hygro-elastic properties for wood biocomposites, which can then exploited in terms of actuation ability, i.e. 4D printing [13].

Indeed, printing thickness not only controls differences of stiffness but also the swelling ability of printed layers (0° and 90°). The differential swelling ratio between active and passive layers decreases from 0.58, 0.43, 0.34 to 0.27% for printing widths of 100, 200, 300% and compressed samples, respectively, which according to bimetallic theory (Eqs. (5)), explains the curvature variation.

The maximal curvature of printed biocomposite systems is around 4 times lower than materials such as Flax/PP hygromorph ($K_{max} = 0.052 \pm 0.008\ mm^{-1}$) [21] with similar thickness ($t \approx 0.4$ mm) but manufactured by compression moulding. This could be explained by lower wood fibre volume (around 15%) in the biocomposite studied here compared to flax/PP stacked film counterparts where the volume fraction reaches 40%. The content of swellable flax fibre in the composite is the driving parameter of the overall swelling process. Thus, increasing this content should improve the actuation ability of biocomposites

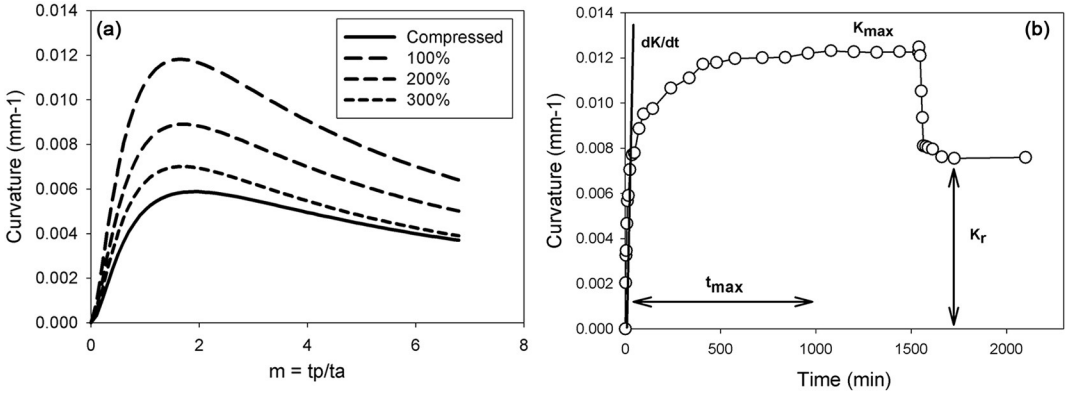

Fig. 7. (a) Curvature variation as a function of thickness ratio *m* for different printing widths. Each printing width has a specific *n* ratio ($n = E_p/E_a$). (b) Typical curvature behaviour as a function of sorption and desorption time, with its defined actuation parameters.

made by FDM. However, high fibre content, and consequently higher melting viscosity, is typically difficult to handle with the FDM device used in this study. The co-development of printing machines and composite formulation should overcome these current problems. Compared to other printed biocomposites (such as Laywoo® filament), lower curvature could be obtained ($K_{max} \approx 0.047\ mm^{-1}$), but only by considering different geometries of printing settings and materials [12]. In addition, no information was provided regarding the sample microstructure. To the best of our knowledge, no other systematic study exists in the literature.

Other comparisons are problematic, especially with bilayers made only of wood, since the experiments are rarely carried out in immersion and also because the layers considered are always thicker (around 5 mm [18] and 1.2 mm [19]), which leads to stiffer actuators. In addition, wood bilayers are naturally composed of swelling tracheid fibres bound together by pectin cements. The overall fibre content within the tissue is thus several times higher than in the biocomposite studied here, which gives the wood bilayers a natural advantage. Fig. 7b shows the typical curvature behaviour of the printed hygromorph biocomposite as a function of sorption and desorption time. Such an actuation mechanism can be characterized by its speed ($\frac{dK}{dt}$), the maximal amplitude K_{max} with its corresponding time t_{max} and the residual curvature after desorption K_r.

Once immersed in water, the hygromorph biocomposite starts swelling and begins to actuate. Maximal curvature is reached after approximately 2500 min for a biocomposite with 100% printing width, while samples prepared with 200 and 300% printing width require less than 1000 min. This trend matches the difference observed for water uptake of biocomposite according to their printing width (Fig. 4a). The microstructure associated with varying porosity, induced by FDM process, could therefore alter the actuation response, since it controls the water uptake mechanism and swelling ratio, i.e. the driving principles. By comparing the values of t_{max} with maximal sorption time (around 40,000 min) (Fig. 4a), we can see that actuation is faster than water absorption when considering a stationary/steady state regime. This implies that samples cease to bend but continue to absorb water. Similar behaviours have been reported with flax/PP hygromorph biocomposites, and are assumed to be linked to mechanosorptive damage mechanisms [21]. The variation of maximal curvature K_{max} as a function of actuation speed (dK/dt) (Fig. 8a) shows that the experimentally determined maximal curvature follows a similar trend to that calculated by bimetallic theory (Fig. 7a). The printing width, the induced hygro-elastic properties and the microstructure influence K_{max} as well as the actuation speed, but with an opposite trend. Increasing printing width (from 100 to 300%) decreases the maximal curvature obtained, while it improves the actuation rate (Fig. 8a).

These observations imply that weak interlayer and interfilament interactions (assumed for samples prepared with 300% printing width) cannot generate sufficient swelling stress to induce high curvature of hygromorph biocomposites, as confirmed by swelling measurements (Fig. 4b). At the same time, the higher porosity could promote water transport and thus enhance the actuation speed. Compared to compression moulding, the FDM process leads to material characteristics which are suitable for a range of moisture-induced biocomposite actuation functionalities and which are associated with improved mechanical properties.

For natural actuators such as pine cones, the sorption mechanism basically depends on liquid water transport driven by capillary forces, while drying is dominated by slow diffusion of water vapour through the pores, which explains the slower desorption phenomena [32]. Here, the desorption and subsequent straightening of a hygromorph biocomposite occurs three time faster than the bending induced by the sorption mechanism, thus confirming the observations of Correa et al. [12]. The water transport mechanism occurring in our biocomposite (i.e. a heterogeneous material with hydrophilic sites and porosity) needs to be clarified by further research. The transformation process is not fully reversible as shown by Fig. 8b. Samples with 100% and 200% printing width allow a curvature recovery of 50%, while 300% printing width and compressed samples show more than 60% curvature recovery after one cycle. Lack of reversibility could be due to mechanosorptive degradation, especially in the wood fibre/polymer matrix interphase area. These issues could be addressed through the optimization of biocomposite formulation by tailoring interfacial bonding strength.

Higher porosity (as in samples prepared with 300% printing width) as well as lower interfilament and interlayer interactions do not lead to a higher degradation rate after one actuation cycle compared to samples prepared with 100 and 200% printing width. Indeed, the difference between samples prepared with 100%, 200% and 300% printing width and compressed samples is explained by the lower bending actuation and thus lower strain of the compressed biocomposite samples (Fig. 8a).

4. Conclusion

In recent years, we have seen a renewed interest in FDM or 3D printing and an impressive development of devices as well as materials. However, very little systematic research has been undertaken on natural-fibre-reinforced composite materials, especially regarding their mechanical behaviour and the influence of the manufacturing parameters used for the printing.

The present study emphasizes that printing width (100, 200 and 300%) influences the mechanical properties of wood biocomposites by modifying their microstructure (porosity). Mechanical parameters are several times lower than the common properties of samples prepared via the compression process. Indeed, the FDM process does not involve pressure levels comparable to those encountered in common extrusion or injection moulding processes. Thus, wood-fibre orientation appears to follow the printing orientation of the filament, while interfilament

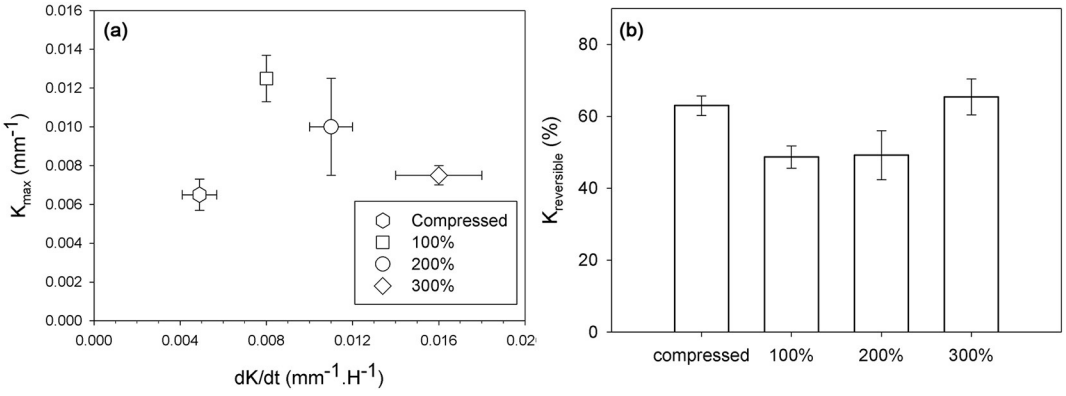

Fig. 8. (a) Maximal curvature (K_{max}) as a function of actuation speed (dK/dt) for different printing widths and compressed samples, and (b) reversible curvature (%) for samples with different printing parameters.

and interlayer interactions could be considered as the weakest link of the printed material. Increasing filament width enhances the porosity but lowers the cohesion of the material. This results in a reduction of tensile strength as well as fast and increased water uptake. The high swelling ratio of wood biocomposites reflects their anisotropic hygroelastic properties, while higher swelling is obtained for printed biocomposites compared to their compressed counterparts. Currently, FDM can produce materials with relatively poor mechanical properties and high hygroscopic sensitivity, which could be considered as a drawback.

However, by applying bio-inspiration from seed dispersal (for example, pinecones), the hygroscopic properties could be turned into an advantage in the design of new kinds of passive hygromorph products. Indeed, by printing a bilayer microstructure mimicking a pinecone, we could generate a programmable moisture-actuated functionality for biocomposites, by following the 4D printing concept. Such a concept was first defined in 2014 [13], but there is still a lack of information on the relationship between the layer-by-layer printing process (FDM) and the actuation properties induced by natural-fibre composites. The comparison of printed samples with compressed counterparts demonstrates that the FDM process provides materials with characteristics that are suitable for a range of moisture-induced actuation functionalities in biocomposites, and with better mechanical properties. Indeed, FDM allows us to improve the maximal curvature and actuation speed of wood biocomposites.

We still require the optimization of biocomposite formulation to improve actuation performance, and especially durability, by tailoring interfacial bond strength as well as the selection of fibre and matrix.

Acknowledgments

We first thank Priscille Bourdilleau for her involvement in this study. Kevin Henry and Yves-Marie Corre from ComposiTIC are also greatly acknowledged for their help. We finally thank Pierre d'Arras from Van Robayes. Michael Carpenter post-edited the English style.

References

[1] O. Faruk, A.K. Bledzki, H.-P. Fink, M. Sain, Biocomposites reinforced with natural fibers: 2000–2010, Prog. Polym. Sci. 37 (2012) 1552–1596, http://dx.doi.org/10.1016/j.progpolymsci.2012.04.003.
[2] A. Bourmaud, C. Baley, Effects of thermo mechanical processing on the mechanical properties of biocomposite flax fibers evaluated by nanoindentation, Polym. Degrad. Stab. 95 (2010) 1488–1494, http://dx.doi.org/10.1016/j.polymdegradstab.2010.06.022.
[3] A. Bourmaud, A. Le Duigou, C. Baley, 14-Mechanical Performance of Flax-based Biocomposites, Biocomposites, Elsevier, 2015 365–399, http://dx.doi.org/10.1016/B978-1-78242-373-7.00013-5.
[4] H. Brooks, S. Molony, Design and evaluation of additively manufactured parts with three dimensional continuous fibre reinforcement, Mater. Des. 90 (2016) 276–283, http://dx.doi.org/10.1016/j.matdes.2015.10.123.
[5] B.N. Turner, R. Strong, S. a Gold, A review of melt extrusion additive manufacturing processes: I. Process design and modeling, Rapid Prototyp. J. 20 (2014) 192–204, http://dx.doi.org/10.1108/RPJ-01-2013-0012.
[6] R. Anitha, S. Arunachalam, P. Radhakrishnan, Critical parameters influencing the quality of prototypes in fused deposition modelling, J. Mater. Process. Technol. 118 (2001) 385–388, http://dx.doi.org/10.1016/S0924-0136(01)00980-3.
[7] L.M. Galantucci, F. Lavecchia, G. Percoco, Quantitative analysis of a chemical treatment to reduce roughness of parts fabricated using fused deposition modeling, CIRP Ann. Manuf. Technol. 59 (2010) 247–250, http://dx.doi.org/10.1016/j.cirp.2010.03.074.
[8] S.S. Crump, Apparatus and Method for Creating Three-dimensional Objects, 1992 15.
[9] S.-H. Ahn, M. Montero, D. Odell, S. Roundy, P.K. Wright, Anisotropic material properties of fused deposition modeling ABS, Rapid Prototyp. J. 8 (2002) 248–257, http://dx.doi.org/10.1108/13552540210441166.
[10] D. Espalin, J. Ramirez, F. Medina, R. Wicker, Multi-material, multi-technology FDM: exploring build process variations, Rapid Prototyp. J. 20 (2014) 236–244.
[11] B.M. Tymrak, M. Kreiger, J.M. Pearce, Mechanical properties of components fabricated with open-source 3-D printers under realistic environmental conditions, Mater. Des. 58 (2014) 242–246, http://dx.doi.org/10.1016/j.matdes.2014.02.038.
[12] D. Correa, A. Papadopoulou, C. Guberan, N. Jhaveri, S. Reichert, A. Menges, et al., 3D printing wood: programming hygroscopic material transformations, 3D Print Addit. Manuf. 2 (2015) 106–116.
[13] S. Tibitts, The Emergence of 4D Printing, TED Talks2013.
[14] D. Raviv, Z. Wei, C. McKnelly, A. Papadopoulou, A. Kadambi, B. Shi, et al., Active printed materials for complex self-evolving deformations, Sci. Rep. 4 (2014) 1–8.
[15] Q. Ge, C.K. Dunn, H.J. Qi, M.L. Dunn, Active origami by 4D printing, Smart Mater. Struct. 23 (2014) 094007, http://dx.doi.org/10.1088/0964-1726/23/9/094007.
[16] M.M. Kabir, H. Wang, K.T. Lau, F. Cardona, Chemical treatments on plant-based natural fibre reinforced polymer composites: an overview, Compos. Part B 43 (2012) 2883–2892, http://dx.doi.org/10.1016/j.compositesb.2012.04.053.
[17] Z.N. Azwa, B.F. Yousif, A.C. Manalo, W. Karunasena, A review on the degradability of polymeric composites based on natural fibres, Mater. Des. 47 (2013) 424–442, http://dx.doi.org/10.1016/j.matdes.2012.11.025.
[18] M. Ruggeberg, I. Burgert, Bio-inspired wooden actuators for large scale applications, PLoS One 10 (2015) 1–16.
[19] A. Holstov, B. Bridgens, G. Farmer, Hygromorphic materials for sustainable responsive architecture, Constr. Build. Mater. 98 (2015) 570–582, http://dx.doi.org/10.1016/j.conbuildmat.2015.08.136.
[20] S. Reichert, A. Menges, D. Correa, Meteorosensitive architecture: biomimetic building skins based on materially embedded and hygroscopically enabled responsiveness, Comput. Des. 60 (2015) 50–69, http://dx.doi.org/10.1016/j.cad.2014.02.010.
[21] A. Le Duigou, M. Castro, Moisture-induced self-shaping flax-reinforced polypropylene biocomposite actuator, Ind. Crop. Prod. 71 (2015) 1–6, http://dx.doi.org/10.1016/j.indcrop.2015.03.077.
[22] C. Dawson, J. Vincent, A. Rocca, How pine cone open, Nature 390 (1997) 668.
[23] I. Burgert, P. Fratzl, Actuation systems in plants as prototypes for bioinspired devices, Philos. Trans. R. Soc. A Math. Phys. Eng. Sci. 367 (2009) 1541–1557.
[24] H. Peltola, E. Pääkkönen, P. Jetsu, S. Heinemann, Wood based PLA and PP composites: effect of fibre type and matrix polymer on fibre morphology, dispersion and composite properties, Compos. A: Appl. Sci. Manuf. 61 (2014) 13–22, http://dx.doi.org/10.1016/j.compositesa.2014.02.002.
[25] L. Sobczak, R.W. Lang, A. Haider, Polypropylene composites with natural fibers and wood – general mechanical property profiles, Compos. Sci. Technol. 72 (2012) 550–557, http://dx.doi.org/10.1016/j.compscitech.2011.12.013.
[26] S. Migneault, A. Koubaa, P. Perré, B. Riedl, Effects of wood fiber surface chemistry on strength of wood–plastic composites, Appl. Surf. Sci. 343 (2015) 11–18, http://dx.doi.org/10.1016/j.apsusc.2015.03.010.
[27] a. Awal, M. Rana, M. Sain, Thermorheological and mechanical properties of cellulose reinforced PLA bio-composites, Mech. Mater. 80 (2015) 87–95, http://dx.doi.org/10.1016/j.mechmat.2014.09.009.
[28] G. Faludi, G. Dora, K. Renner, J. Móczó, B. Pukánszky, Improving interfacial adhesion in PLA/wood biocomposites, Compos. Sci. Technol. 89 (2013) 77–82, http://dx.doi.org/10.1016/j.compscitech.2013.09.009.
[29] A. Le Duigou, A. Bourmaud, P. Davies, C. Baley, Long term immersion in natural seawater of Flax/PLA biocomposite, Ocean Eng. 90 (2014) 140–148, http://dx.doi.org/10.1016/j.oceaneng.2014.07.021.
[30] W.V. Srubar, C.W. Frank, S.L. Billington, Modeling the kinetics of water transport and hydroexpansion in a lignocellulose-reinforced bacterial copolyester, Polymer (Guildf) 53 (2012) 2152–2161, http://dx.doi.org/10.1016/j.polymer.2012.03.036.
[31] T. Joffre, E.L.G. Wernersson, A. Miettinen, C.L. Luengo Hendriks, E.K. Gamstedt, Swelling of cellulose fibres in composite materials: constraint effects of the surrounding matrix, Compos. Sci. Technol. 74 (2013) 52–59, http://dx.doi.org/10.1016/j.compscitech.2012.10.006.
[32] E. Reyssat, L. Mahadevan, Hygromorph: from pine cone to biomimetic bilayers, J. R. Soc. 6 (2009) 951–957.
[33] R. Erb, J. Sander, R. Grisch, A. Studart, Self-shaping composites with programmable bioinspired microstructures, Nat. Commun. 4 (2013) 1–8.
[34] A. Le Duigou, A. Kervoelen, A. Le Grand, M. Nardin, C. Baley, Interfacial properties of flax fibre-epoxy resin systems : existence of a complex interphase, Compos. Sci. Technol. 100 (2014) 152–157.